Developmental Cell, Vol. 7, 801–814, December, 2004, Copyright ©2004 by Cell Press

The Oxidative Burst at Fertilization Is Dependent upon Activation of the Dual Oxidase Udx1

Julian L. Wong, Robbert Créton, and Gary M. Wessel*
Department of Molecular Biology, Cell Biology, and Biochemistry
Box G
Brown University
Providence, Rhode Island 02912

Summary

The sea urchin egg is a quiescent cell…until fertilization, when the egg is activated. The classic respiratory burst at fertilization is the result of prodigious hydrogen peroxide production, but the mechanism for this synthesis is not known. Here we quantitate the kinetics of hydrogen peroxide synthesis at a single-cell level using an imaging photon detector, showing that 60 nM hydrogen peroxide accumulates within the perivitelline space of each zygote. We find that the NADPH oxidation activity is enriched at the cell surface and is sensitive to a pharmacological inhibitor of NADPH oxidase enzymes. Finally, we show that a sea urchin dual oxidase homolog, Udx1, is responsible for generating the hydrogen peroxide necessary for the physical block to polyspermy. Phylogenetic analysis of the enzymatic modules in Udx1 suggests a potentially conserved role for the dual oxidase family in hydrogen peroxide production and regulation during fertilization.

Introduction

Eggs are often bombarded by innumerable sperm. All but one—the first to fuse with the egg—must be repelled from the surface to prevent the lethal condition of polyspermy. The embryo meets this challenge by rapidly modifying its cell surface and extracellular matrix. Multiple variations to this modification are found throughout phylogeny (reviewed in Shapiro et al., 1989; Wessel et al., 2001).

The block to polyspermy in sea urchins involves a dramatic biochemical transformation of the egg extracellular matrix, the vitelline layer, to a histologically distinct embryonic matrix, the fertilization envelope (FE). The driving force of this transition is secretion of the cortical granules. At least three discrete steps are involved with the formation of this extracellular barrier. (1) Following cortical granule exocytosis, an autoactivating serine protease severs plasma membrane attachments to the egg's vitelline layer, allowing the separation of this matrix from the egg surface (Haley and Wessel, 1999, 2004). (2) The structural components of the FE, primarily derived from the cortical granules (reviewed in Wessel et al., 2001; Wong and Wessel, 2004), self-assemble into the vitelline layer scaffold and form a distinct pattern of interwoven fibers (Chandler and Heuser, 1980). (3) The cortical granule-derived enzyme ovoperoxidase is targeted to the FE by the tethering protein proteoliaisin (Somers et al., 1989). As the structural proteins self-polymerize into fibers, ovoperoxidase activity increases in response to alkalization (Deits and Shapiro, 1986) as synthesis of one of its substrates, hydrogen peroxide (H_2O_2), increases (Foerder et al., 1978; Heinecke and Shapiro, 1989). The catalytic activity of ovoperoxidase peaks within 5 min following fertilization, resulting in the formation of covalent *o*-*o*-di-tyrosine bonds between FE proteins (Foerder and Shapiro, 1977; Hall, 1978; Nomura and Suzuki, 1995). These cross-links brace the fibrous network into a solid structure, "hardening" it to protect the embryo (Shapiro et al., 1989).

An essential substrate for ovoperoxidase, and a likely component involved with cell signaling, H_2O_2 is produced by a calcium-dependent mechanism involving the reduction of one molecule of oxygen and the oxidation of two proton donors—hereby referred to as "oxidase activity"—whose peak output occurs at about 7–8 min postfertilization (Foerder et al., 1978; Heinecke and Shapiro, 1989). This temporal correlation between peak H_2O_2 production and ovoperoxidase activity is not coincidental; both have likely evolved in a tightly regulated system in order to limit the potentially lethal effects of H_2O_2 on the embryo without compromising FE integrity.

The existence of oxidase activity was first documented while measuring oxygen consumption following fertilization (Warburg, 1908). Although originally ascribed to oxidative phosphorylation—hence its misnomer as a "respiratory burst"—the majority of the oxygen consumed was later attributed to the synthesis of H_2O_2. This phenomenon was subsequently likened to the respiratory burst associated with activated neutrophils (Klebanoff et al., 1979; Heinecke and Shapiro, 1992). Neutrophils use a complex of intramembraneous and cytosolic proteins to regulate the oxygen reductase activity of their main player, cytochrome b_{558}, a heterodimeric complex of $p22^{PHOX}$ and $gp91^{PHOX}$ (reviewed in Babior, 1999). The H_2O_2 synthesized by the neutrophil is used by myeloperoxidase to synthesize the hypochlorous acid (HOCl) that kills bacteria (reviewed in Pullar et al., 2000).

We sought to characterize the respiratory burst activity during fertilization in two species of sea urchins. The results of our experiments suggest that the redox machinery responsible for the rapid oxygen consumption following fertilization is evolutionarily distinct from the neutrophil NADPH oxidase system. We show instead that a dual oxidase, Udx1, is responsible for the H_2O_2 synthesis at fertilization.

Results

Quantitation of Hydrogen Peroxide Production in Single Eggs at Fertilization

We quantitated hydrogen peroxide (H_2O_2) production on a single-cell level using luminol and an imaging photon

*Correspondence: rhet@brown.edu

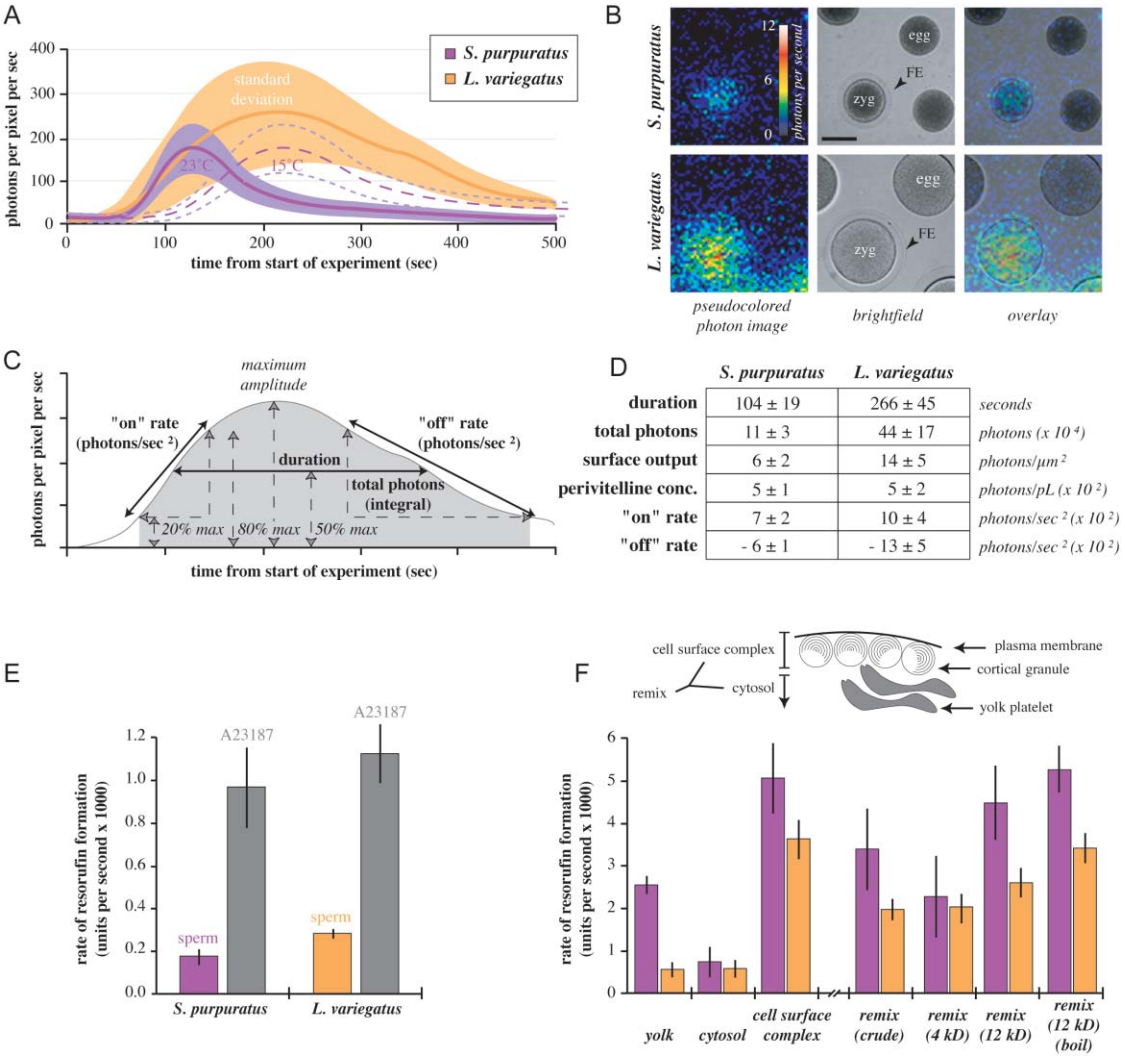

Figure 1. Characteristics of the Oxidative Burst

(A) Mean (line) profiles of total photon output in *Strongylocentrotus purpuratus* and *Lytechinus variegatus* zygotes. Standard deviation over 10 zygotes from 4 females is reported as background shading. Dashed trace represents the transformed profile of *S. purpuratus* zygotes fit to events at 15°C (Foerder et al., 1978)—note the conservation in traces between traces of each species after.

(B) Images of H_2O_2 output from individual eggs. Brightfield images (middle) show the eggs (egg) and zygotes (zyg) 500 s after insemination. Note the fertilization envelope (FE) of the zygote. Pseudocolored images (left) represent photons collected over a 50 s window. The graded color scale represents 0 (black) to 12 (white) photons per pixel per second. Scale bar equals 50 μm.

(C) Schematic trace indicating measurements used to calculate the average duration, total photon output at 20% maximum amplitude, "on" and "off" rates of the detected oxidative burst.

(D) Tabulated measurements per zygote per species. All photon data represents absolute quantities, after optical and calibration correction of detected data.

(E) Species comparison of the rates of H_2O_2 production upon fertilization (color) or activation with the ionophore A23187 (gray) on egg populations, as measured with resorufin formation.

(F) Egg fractions (5 μg total protein of *S. purpuratus*; 10 μg of *L. variegatus*) tested for an ability to generate resorufin in a calcium-dependent fashion. Vertical lines indicate standard deviation. All pairwise differences between fraction data are significant ($p \leq 0.01$) with the exception of the following: *L. variegatus* yolk-to-cytosol ($p = 0.16$), cell surface complex-to-boil ($p = 0.12$), crude-to-4 kDa ($p = 0.77$); *S. purpuratus* cell surface complex-to-12 kDa ($p = 0.24$), cell surface complex-to-boil ($p = 0.64$), crude-to-4 kDa ($p = 0.07$), and crude-to-12 kDa ($p = 0.07$).

detector (IPD) system (Takahashi et al., 1989; Créton and Jaffe, 2001). Such a chemiluminescent reporter activity is peroxidase dependent during sea urchin fertilization (Foerder et al., 1978; Takahashi et al., 1989), so we initially measured H_2O_2 production in the presence or absence of exogenous horseradish peroxidase (HRP) to test whether H_2O_2 synthesis or ovoperoxidase would be the limiting component toward detection. Eggs do not produce detectable H_2O_2 (Figure 1B), whereas the prodigious levels of H_2O_2 detectable in fertilized eggs is the same with or without HRP (data not shown), suggesting that the limiting step during fertilization is H_2O_2 production and not ovoperoxidase activity. Thus, all subsequent measurements were made relying on endogenous ovoperoxidase to catalyze the H_2O_2-specific chemiluminescent reaction.

When corrected for the quantum efficiency of luminol conjugation with H_2O_2 (1.24%; Créton and Jaffe, 2001), *Strongylocentrotus purpuratus* zygotes produce $9 \pm 3 \times 10^6$ molecules of H_2O_2 while *Lytechinus variegatus* generates $36 \pm 14 \times 10^6$ molecules of H_2O_2 per zygote (Figure 1D). When normalized to the volume of the perivitelline space, the region between the plasma membrane and the fertilization envelope (FE) where active ovoperoxidase is present (Somers et al., 1989; LaFleur et al., 1998), the final H_2O_2 concentration between the two species is equal: 60 ± 17 nM H_2O_2 per *S. purpuratus* and 65 ± 25 nM H_2O_2 per *L. variegatus* zygote. Transformation of the trace of *S. purpuratus* zygotes at 23°C to 15°C (Foerder et al., 1978) yields a profile nearly identical to that of *L. variegatus* (Figure 1A, dashed trace), supporting evolutionary conservation of the oxidative burst.

Kinetics of the Respiratory Burst in Populations of Eggs

Our observations with the IPD showed little variation between individual zygotic rates of H_2O_2 synthesis (Figure 1). The spatial-temporal power of this microscopic observation, however, greatly limits the throughput of data collection. We therefore developed a microtiter plate assay to measure real-time kinetics of the oxidative burst for egg populations. We used the peroxidase-dependent oxidation of Amplex Red to resorufin as a proxy to track the kinetics of H_2O_2 generation in vivo during fertilization. One systemic limitation to the accuracy of these measurements, as in the IPD system, is the competition for free H_2O_2 between endogenous ovoperoxidase protein targets versus Amplex Red. Thus, while both IPD and microtiter techniques provide an estimation of H_2O_2 produced, each is an underestimation due to this competition.

Using this assay, we observe a significant difference between the oxidase activity from fertilized zygotes compared to A23187-activated eggs from both *S. purpuratus* and *L. variegatus* (Figure 1E). Ionophore activation caused a near-linear accumulation of resorufin over the course of the experiment while the fertilization response of the zygotes was biphasic (Supplemental Figure S1 at http://www.developmentalcell.com/cgi/content/full/7/6/801/DC1/). Our explanation of this kinetic difference is that ionophore acts instantaneously and uniformly over the egg whereas sperm initiates a polarized wave of activation. Due to the additional pleiotropic effects of calcium ionophore treatment on the egg, we chose to limit our analysis of H_2O_2 production to fertilized eggs, but note that these data show that free cytosolic calcium is sufficient to achieve an oxidative burst in vivo.

Biochemical Localization of the Oxidative Burst Activity

We sought to locate the source of the oxidase activity by fractionating the cell into cell surface complex, consisting of the egg plasma membrane and its associated cortical granules (Kinsey, 1986), yolk (Brooks and Wessel, 2002), and cytosol. Using an adaptation to our microtiter plate protocol, we measured the H_2O_2 production following calcium activation of a partially reconstituted system containing exogenous NADPH and active protein kinase C (Heinecke and Shapiro, 1989, 1992). The majority of enzymatic activity is associated with the cell surface complex (Figure 1F). Recombination of egg cytosol with cell surface complex, however, inhibits the conversion of Amplex Red to resorufin. We hypothesized that this loss of detectable H_2O_2 is due to the scavenging activity of catalase, glutathione peroxidase (Fahey et al., 1976), and/or ovothiol (Turner et al., 1986, 1988). We tested this model by dialyzing compounds from cytosol using 4 or 12 kDa permeability limits. More activity from these recombined fractions was achieved as larger molecules were dialyzed out, but full recovery of activity was not achieved until the 12 kDa dialyzed cytosol was boiled for 10 min (Figure 1F). These results suggest that an unknown, proteinaceous factor may be regulating the cell surface oxidase in vivo.

Class-Specific Pharmacological Inhibition of the Oxidative Burst

We treated both *S. purpuratus* and *L. variegatus* eggs with three inhibitors of the neutrophil respiratory burst complex representing two different structural classes. Diphenyleneiodonium (DPI) is a potent inhibitor of both the neutrophil oxidative burst and endothelial nitric oxide synthase, with half-maximum inhibitory concentrations (IC_{50}) of 3–6 μM (O'Donnell et al., 1993; Wang et al., 1993). Apocynin (Apo; 4′-hydroxy-3′-methoxyacetophenone), and its ester analog acetosyringone (Aceto; 3′, 5′-dimethoxy-4′-hydroxyacetophenone), have been shown to inhibit the neutrophil respiratory burst with IC_{50} of 10 and 4 μM, respectively (Van den Worm et al., 2001).

The efficacy of each inhibitor on the oxidative burst at fertilization is split based on its class (Figure 2A). Consistent with reports for neutrophils (O'Donnell et al., 1993; Wang et al., 1993), concentrations near 3 μM DPI yield half-maximal H_2O_2 output in the sea urchin zygote measured in a population or individually with the IPD (Figure 2B). In contrast, even 10-fold higher than IC_{50} concentrations of the phenolic compounds Apo and Aceto do not affect the rate of H_2O_2 production. The variance observed at these high Apo and Aceto concentrations is likely a consequence of pleiotropic effects on the zygotes.

We next tested if these inhibitors affected the activity associated with the isolated cell surface complex in a similar pattern. In both urchin species tested, DPI and Aceto, but not Apo, resulted in a dose-dependent inhibition of cell surface complex activity (Figure 2C). When used together, DPI and Aceto further inhibited H_2O_2 production, suggesting that their additive effects are a result of targeting different machinery. Thus, in combination with our in vivo observations, these data suggest that the egg oxidative burst uses a mechanism distinct from the neutrophil $gp91^{PHOX}$ system.

Identification of an Egg Dual Oxidase

A search of the Sea Urchin Genome Project database yielded one *S. purpuratus* exon sequence that matched the sequence of a thyroid oxidase; no other homologs have been identified in the genome or by degenerate PCR screens to date (data not shown). The *L. variegatus* ortholog of this exon was cloned in full and determined

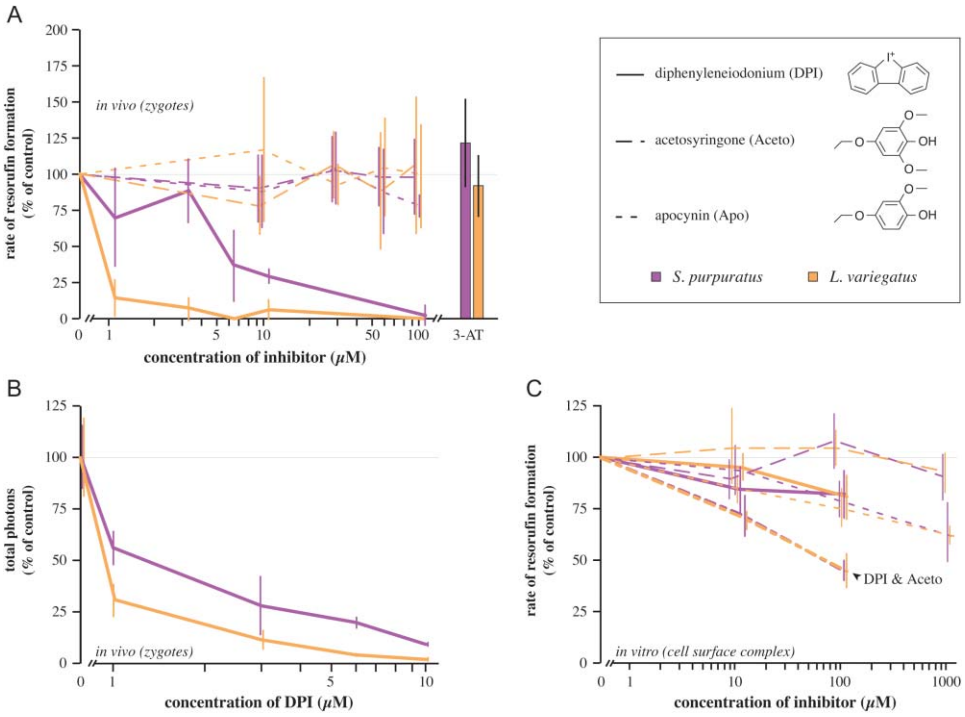

Figure 2. Effects of Pharmacological Inhibitors of the Neutrophil Respiratory Burst on the Oxidative Burst at Fertilization

(A) H_2O_2 production from about 100 zygotes measured by the formation of resorufin after pretreatment with inhibitors. The effects of 1 mM 3-AT are reported as a control (bar).

(B) Effect of DPI on total photon output using the IPD.

(C) The effects of each inhibitor on H_2O_2 production in cell surface complex on resorufin formation.

In all graphs, concentrations along the x axis are reported in logarithmic scale; vertical bars represent the standard deviation for each concentration tested.

to be a member of the dual oxidase family of transmembrane proteins. Further comparison to available *S. purpuratus* genome sequence also identified select regions of homology between the two species (Supplemental Figure S2). The overall organization of the sea urchin oxidase is identical to the other dual oxidases described (Lambeth, 2002), with an N-terminal peroxidase domain and a C-terminal reductase domain linked by a cytoplasmic bridge with two EF hands (Figure 3A), suggesting that calcium may regulate these enzymes (Lewit-Bentley and Rety, 2000). We now refer to this dual oxidase as "urchin dual oxidase 1" (Udx1), but it is also registered in GenBank as "duox1.urchin" to follow the current nomenclature (Lambeth, 2002).

A single 6 kb *Udx1* transcript (Figure 3B) accumulates specifically in developing oocytes (Figure 3C), supporting the hypothesis that the Udx1 protein is present in eggs. By a more sensitive multiplex-reverse transcriptase PCR amplification, we found the *Udx1* mRNA is present in all stages of oocytes, eggs, and zygotes, whereas the cortical-granule-specific transcript *SFE9* is present only in developing oocytes (Figure 3D; Wessel, 1995).

We generated separate polyclonal antibodies against the peroxidase, cytoplasmic bridge, and cytoplasmic NADPH binding carboxyl terminus domains of Udx1 to localize the protein. Immunoblot analysis identified a 185 kDa protein, and its proteolyzed fragments, from all egg fractions tested (Figure 3E), identical to the 185.7 kDa protein predicted from the open reading frame. Consistent with the kinetic localizations, Udx1 is present at the egg cell surface. Surprisingly, Udx1 protein is even more abundant in yolk-enriched fractions, consistent with the granular staining in the oocytes, eggs, and zygotes (Figures 3F–3N) but not predicted quantitatively by oxidase activity assays (Figure 1F). This oxidase activity in the yolk-enriched fraction implies that a pool of Udx1 may be kept inactive in eggs, perhaps through the same unidentified factors found in the cytosolic fractions above (Figure 1F).

Udx1 Generates the Oxidative Burst Following Fertilization

The cortical localization of Udx1 in the egg makes it a prime candidate to be the DPI-sensitive enzyme. To test this, we asked whether the polyclonal antibodies against the dual oxidase could inhibit H_2O_2 synthesis in zygotes. In vitro incubation of cell surface complex with antibodies inhibited H_2O_2 synthesis when compared to equal concentrations of preimmune IgGs (Figure 4B). The greatest inhibition was observed from 100 μg/ml of the anti-NADPH antibodies; pairing antibodies to other domains with this concentration of anti-NADPH antibody did not significantly improve the inhibitory phenotype. The 30% inhibition of H_2O_2 synthesis achieved using antibodies is only slightly better than with DPI.

We extended these inhibition experiments in vivo by injecting anti-NADPH domain antibodies into eggs and

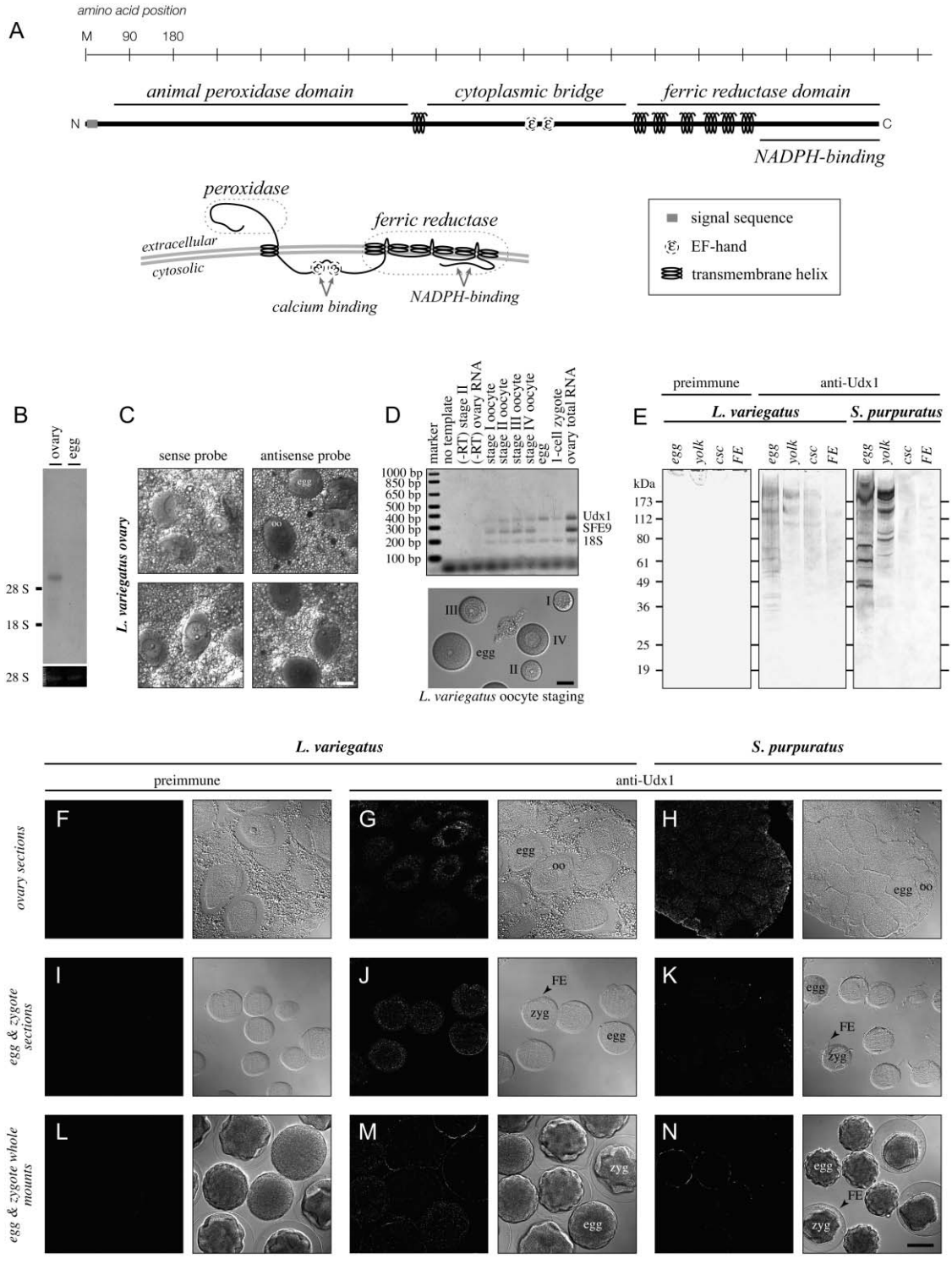

Figure 3. Udx1 Is Expressed in Eggs and Zygotes

(A) Schematic diagrams of the dual oxidase.

(B) RNA blot probed for Udx1 in ovary and egg total RNA (10 μg each). Ethidium bromide staining of 28S rRNA is shown as a loading control.

(C) Ovary whole-mount in situ hybridization of *Udx1*.

(D) Multiplex, reverse transcriptase (RT) polymerase chain reaction from whole-cell lysates derived from different stages of oogenesis or zygotes. Staging was scored based on the nuclear-to-cytoplasmic ratios (DIC image).

(E) Immunoblots of egg fractions probed with 2 μg/ml each antibody or 6 μg/ml preimmune IgGs. The following mass of total protein was loaded: *L. variegatus*, 100 μg egg, 25 μg yolk or cell surface complex, 20 μg soft fertilization envelope (FE); *S. purpuratus*, 200 μg egg, 50 μg yolk or cell surface complex, 40 μg soft fertilization envelope (FE).

(F–N) Immunofluorescence on tissue sections of ovary, eggs, or zygotes (F–K) and on whole-mount eggs or zygotes (L–N). All samples probed with 100 μg/ml preimmune (F, I, L) or a mix of 30 μg/ml of each Udx1 antibody (G, H, J, K, M, N). Oocytes (oo), eggs (egg), zygotes (zyg), and fertilization envelope (FE) are indicated. Scale bars equal 50 μm.

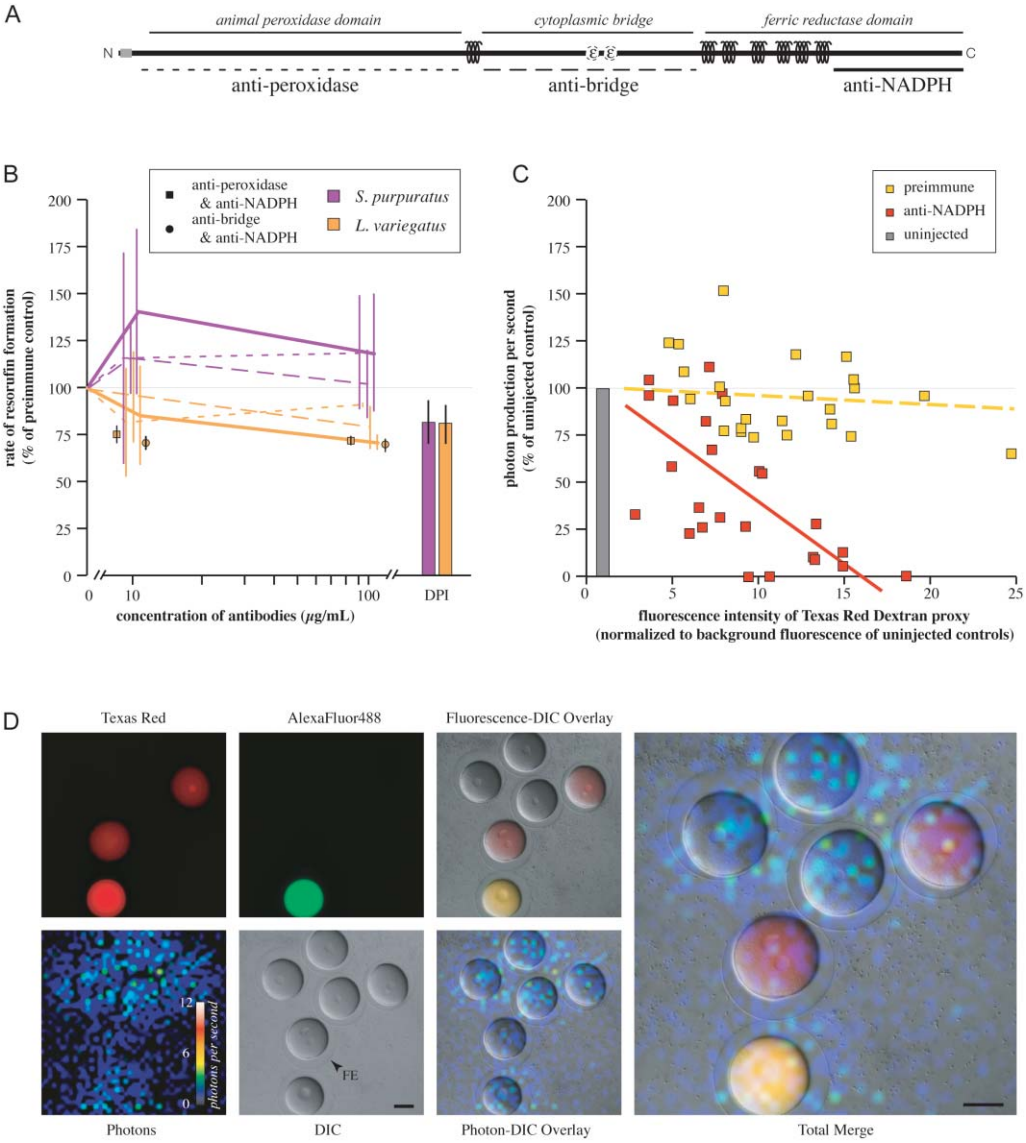

Figure 4. Antibodies against the Dual Oxidase Domains Inhibit H_2O_2 Production

(A) Diagram of Udx1 immunogens.

(B) Effects of antibodies on cell surface complex H_2O_2 production reported as the percentage of preimmune control at the same total concentration. Bars represent inhibition achieved with 100 μM DPI. Concentrations along the x axis are reported in logarithmic scale; vertical bars represent the standard deviation.

(C) Effect of injected anti-NADPH or preimmune antibodies on photon output, presented as percentage of uninjected controls. Antibody concentrations are reported as normalized Texas red fluorescence.

(D) The H_2O_2 output in a field of zygotes containing three uninjected controls, two anti-NADPH-injected eggs (red), and one preimmune-injected egg (green individual/yellow merge). Individual fluorophore emissions are shown, with corresponding merged image over the DIC image acquired following fertilization (note fertilization envelopes). Pseudocolored images represent total photons collected over a 1200 s window. The graded color scale represents 0 (black) to 12 (white) photons per pixel per second. Oxidative bursts of each zygote are shown in merged images (photon-merge; total merge). Scale bar equals 50 μm.

then measuring the total number of H_2O_2 molecules generated per zygote using the IPD (Figure 4C). Treatments show a wide range of inhibition at lower concentrations of anti-NADPH antibodies, but minor variance at higher concentrations. At the highest concentrations—the range of 12–14 normalized Texas red fluorescence units, or 100 μg/ml of antibody within the egg (calibrations not shown)—H_2O_2 output is completely abolished. This dose-dependent response is in stark contrast to injection of similar amounts of preimmune immunoglobulins. Thus, we believe Udx1 is responsible for the respiratory burst at fertilization.

Biochemical Characterization of the Hydrogen Peroxide Synthesizing Machinery

We next asked how Udx1 is regulated, particularly in light of the inactive reserve found in eggs (see above). Previous work suggested that free calcium, NADPH, and active protein kinase C (PKC) are sufficient for activity,

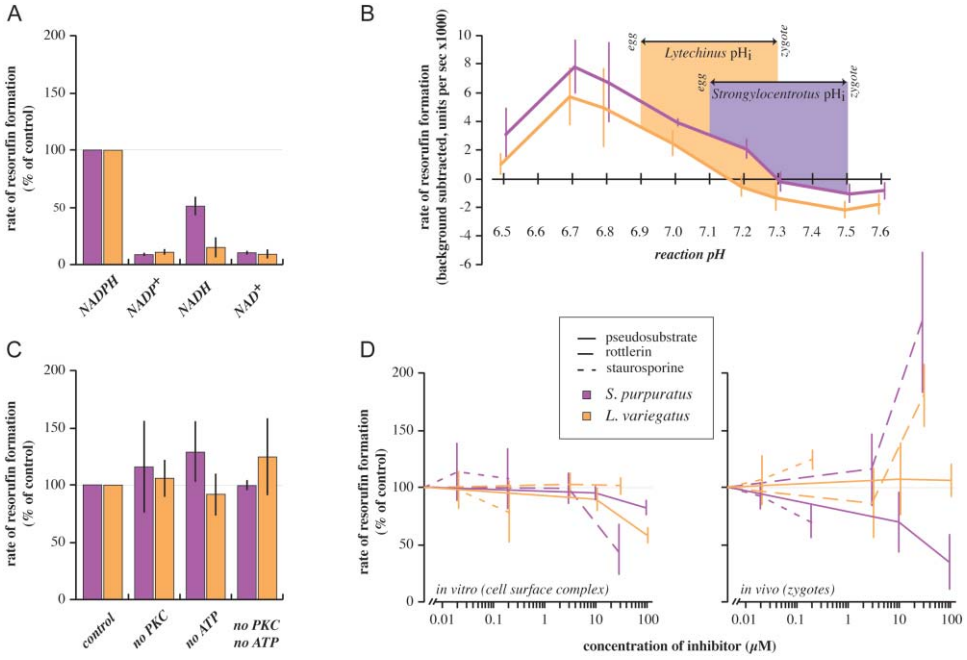

Figure 5. Control of Hydrogen Peroxide Synthesis

(A) Effects of substituting different nicotinamide adenine dinucleotide cofactors on H_2O_2 synthesis rates in cell surface complex. Rates for each treatment are normalized to NADPH control.

(B) Hydrogen peroxide synthesis from cell surface complex is dependent on pH. Shaded regions indicate the range of alkalization that occurs in each sea urchin genus at fertilization (Shen and Steinhardt, 1979; Johnson and Epel, 1981).

(C) Effects of removing exogenous PKC and ATP from the cell surface complex on H_2O_2 synthesis. Rates for each treatment are normalized to control reactions containing all factors. None are significantly different from control ($p > 0.20$).

(D) Effects of inhibiting endogenous protein kinases in cell surface complex (left) or fertilized eggs (right). Concentrations along the x axis are reported in logarithmic scale; vertical bars represent the standard deviation.

the latter requiring exogenous ATP (Heinecke and Shapiro, 1989, 1992). In our system, the sea urchin oxidase prefers the cofactor NADPH to the unphosphorylated NADH (Figure 5A), consistent with previously published observations (Heinecke and Shapiro, 1989) and with the rise in the NADPH:NADH ratio found in echinoid eggs following fertilization (Schomer and Epel, 1998). Hydrogen peroxide production in vitro is not, however, dependent on exogenous PKC or ATP (Figure 6B). If endogenous, membrane bound PKC is necessary for oxidase activity, then PKC inhibitors should affect the kinetics of H_2O_2 synthesis. The sensitivity of oxidase activity to PKC inhibitors—such as rottlerin (Gschwendt et al., 1994; Mellor and Parker, 1998), a myristoylated PKC pseudosubstrate peptide (Eichholtz et al., 1993; Ward and O'Brian, 1993), or the general calcium-dependent protein kinase inhibitor staurosporine (Tamaoki et al., 1986)—is species specific: *S. purpuratus* cell surface complex and zygotes are sensitive to all PKC inhibitors whereas *L. variegatus* is not (Figures 5C and 5D). The instances when oxidase hyperactivity is observed, such as with rottlerin, may be due to pleiotropic effects of the drug itself (Gschwendt et al., 1994).

So what might control the oxidative burst in *L. variegatus*? We tested whether the rise in intracellular pH (pH_i) upon egg activation (Shen and Steinhardt, 1978; Johnson and Epel, 1981) might play a role in Udx1 regulation. In both species, we observed maximal activity between pH 6.7 and 6.9 (Figure 5B), a slightly more acidic profile compared to that observed on ammonium sulfate-extracted egg fractions (Heinecke and Shapiro, 1989). Our pH-dependent activity titrations overlap the temporal rise in pH_i that occurs following fertilization: in *S. purpuratus*, the change in pH_i rises from 7.1 to 7.5, versus *L. pictus*, a close relative of *L. variegatus*, where pH_i rises from pH 6.9 to 7.3 (Shen and Steinhardt, 1978; Johnson and Epel, 1981). Aligning previously published data on calcium and pH_i dynamics with our IPD traces, the overlap suggests a causal relationship. The NADPH oxidase is activated during the first 5 min following fertilization and then shuts down over the next 5 min (Figure 1A). This initial H_2O_2 production corresponds to the rise in intracellular calcium concentration (Shen, 1995; Jaffe et al., 2001), while the suppression phase coincides with the plateau of pH_i (Shen and Steinhardt, 1978; Johnson and Epel, 1981) and active membrane retrieval (Whalley et al., 1995). Our observation that maximal oxidase activity in vitro is more acidic than found in vivo implies that physiologic pH_i may repress Udx1 activity. This global data on pH_i does not preclude the possibility that local acidity, perhaps through proton leakage through the animal reductase domain (Schwarzer et al., 2004), could transiently enhance or prolong activity. Alternatively, the modulating effects of pH_i may be dwarfed by calcium affinities or PKC-dependent phosphorylation in the hierarchy of Udx1 regulation.

Inhibition of the Oxidative Burst Impairs Fertilization Envelope Cross-Linking

To test if Udx1 activity is the source of H_2O_2 necessary for ovoperoxidase activity, we measured the impact of

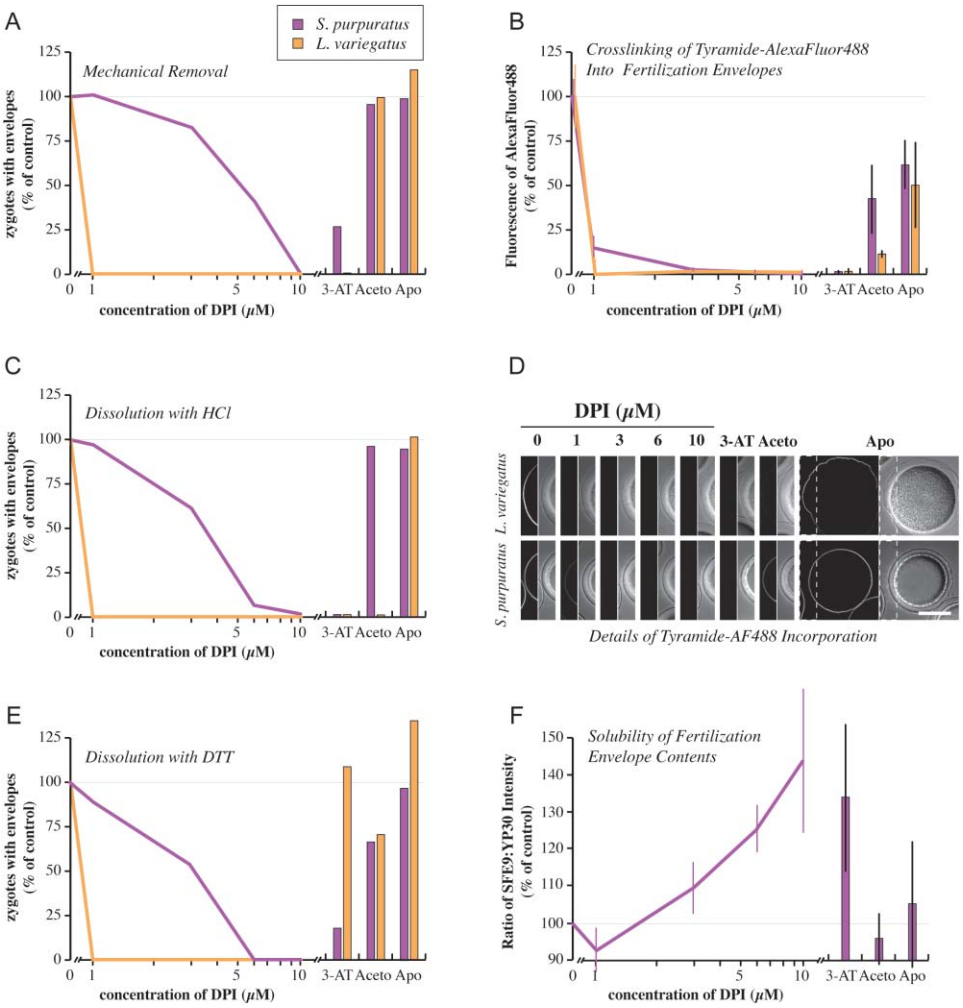

Figure 6. Fertilization Envelope Phenotype Depends on the Oxidative Burst

(A, C, and E) Zygotes exposed to inhibitors were scored for fertilization envelopes (FEs) following (A) mechanical shearing, (C) 6N HCl, or (E) 10 mM dithiothreitol (DTT) exposure.

(B) Incorporation of tyramide-AlexaFluor488 into individual FEs (11–15 zygotes per treatment) formed in the presence of inhibitors.

(D) Typical images of individual zygotes used to quantitate tyramide-AlexaFluor488 incorporation into FEs. Fluorescence images with corresponding DIC images to the immediate right. Scale bar equals 50 μm.

(F) SFE9 cross-linking, normalized to freely soluble YP30, is dependent on oxidase activity.

Per graph, concentrations along the x axis are reported on a logarithmic scale; vertical bars represent standard deviation. Controls of 1 mM 3-AT, 100 μM Aceto, and 100 μM Apo are included.

pharmacological inhibition on the integrity of the final FE. Directly interfering with ovoperoxidase activity results in the loss of FE cross-linking, as observed with 3-amiotriazole (3-AT; Showman and Foerder, 1979). The FE still forms but can be readily removed from the zygote by mild shearing force. In the presence of DPI, 30 min of turbulence denuded zygotes of their FEs (Figure 6A). Similarly, DPI causes the loss of chemical resistance to 6 N hydrochloric acid (HCl) and 10 mM dithiothretiol (DTT) (Figures 6C and 6E). Retention of the FE in the presence of the phenolic compounds Apo and Aceto show that Udx1 alone is responsible for H_2O_2 production.

We supplement these functional tests with an analysis of the degree of protein cross-linking in the FE structural proteins following exposure to these inhibitors. Di- and trityrosine cross-links are formed in the FE (Hall, 1978; Nomura and Suzuki, 1995), probably via a free radical intermediate created by peroxidases (Yip, 1966). Accordingly, this peroxidase-specific mechanism allows for the potential incorporation of free tyrosine analogs to target proteins in the FE (Deits et al., 1984). To measure the impact of the above NADPH oxidase inhibitors on endogenous ovoperoxidase-dependent cross-linking activity, we used tyramide-AlexaFluor488 as an ovoperoxidase substrate (Hunyady et al., 1996). Incorporation of the fluorochrome into the FE acts as a proxy to quantitate the relative number of dityrosine cross-links formed, a measurement that can be used to extrapolate ovoperoxidase activity and, ultimately, net H_2O_2 utilization. Incorporation of the fluorochrome occurs

within 20 min postinsemination, is specific to the FE (Figure 6D), and is abolished when zygotes are exposed to DPI or 3-AT (Figure 6B), supporting the model that Udx1 activity is essential for FE maturation.

We observed a similar depletion of FE protein cross-linking biochemically using the marker SFE9, a structural protein cross-linked into the FE in a time-dependent manner (Wessel, 1995). At fertilization, SFE9 is sufficiently soluble to enter a standard SDS-polyacrylamide gel, whereas protein from mature FEs does not because it is cross-linked into the FE. SFE9 isolated from FEs in the presence of 3-AT is fully soluble. Consistent with all previous data, DPI enhances the soluble-SFE9 phenotype, indicative of a loss in FE cross-linking (Figure 6F).

Discussion

The oxidative burst of fertilization was originally believed to be the result of an increase in respiration reflecting the transition from a quiescent egg to an active zygote (Warburg, 1908). While a fraction of this oxygen is directly attributed to oxidative phosphorylation, the majority of the oxygen consumed is instead converted directly to hydrogen peroxide (H_2O_2) by an egg oxidase activity (Foerder et al., 1978). We now ascribe this H_2O_2 generation to the dual oxidase Udx1.

Why would a dual oxidase be favored for zygotic oxidase activity over the multitude of other animal reductases? One key feature might be its paradoxical and modular functions. Phylogenetic analysis of each catalytic domain (Figure 7A) shows that the dual oxidase animal reductase domain is most closely related to the yeast ferric reductase FRE while its peroxidase is most similar to catalase, an enzyme responsible for the neutralization of H_2O_2 to H_2O and O_2 (Chance, 1949). Our tree suggests that the enzymatic domains of the dual oxidases also have opposing activities: calcium-dependent, pH-sensitive activation of the animal reductase domain converts extracellular O_2 to H_2O_2 (Dupuy et al., 1988). Meanwhile, the catalase-like peroxidase domain could reverse this process to neutralize the toxic reactive oxygen species (ROS) before it can penetrate the cell. The benefits of this antagonism can be seen by comparing the H_2O_2 production of thyrocytes and eggs, both utilizing dual oxidases, to mammalian neutrophils, utilizing $gp91^{PHOX}$/NOX cytochromes (Figure 7B): in thyrocytes, the calcium-sensitive $p138^{Tox}$/Duox2 generates H_2O_2 necessary for a lumenal thyroid peroxidase to conjugate iodide ions to tyrosine residues on thyroglobulin, generating an active hormone that regulates metabolism (reviewed in Dunn and Dunn, 2001). In the sea urchin egg, Udx1 is primarily responsible for generating H_2O_2 necessary for ovoperoxidase-dependent cross-linking of fertilization envelope (FE) proteins, thereby completing a competent block to polyspermy (Hall, 1978; Showman and Foerder, 1979), although the H_2O_2 generated can be spermicidal alone (Boldt et al., 1981; Coburn et al., 1981) or in combination with free halides and active peroxidases (Klebanoff et al., 1979; Schuel and Schuel, 1986). In thyrocytes and fertilized eggs, both normally irreplaceable and nonrenewable cell types (Kimura et al., 2001; Wendl et al., 2002), the dual oxidase's catalase domain may be a first defense against H_2O_2 that diffuses toward the cell surface. A common second defense is cytoplasmic enrichment in ROS scavengers such as cytoplasmic catalase, glutathione, and glutathione peroxidase or its functional equal, ovothiol (Fahey et al., 1976; Turner et al., 1988; Ekholm and Bjorkman, 1997). Neutrophils, on the other hand, directly synthesize superoxide anions (O_2^-) that dismutate to H_2O_2 within the phagosome, where is it used to destroy foreign invaders (Babior, 1999; Pullar et al., 2000; Lambeth, 2002). The intracellular concentration of H_2O_2 reaches toxic levels, resulting in self-destruction—an acceptable outcome considering that the pathogen is eradicated, the neutrophil is replenished by hematopoetic stem cells, and macrophages clear the resultant debris. The insignificance of variable cytosolic glutathione peroxidase activity on neutrophil performance is also consistent with the dispensability of these cells (Bass et al., 1977). Thus, the net diffusion of H_2O_2 away from the cell surface by dual oxidases, versus a self-destructive phenotype, is favorable for periodically stimulated cells that must remain viable throughout an organism's life. Our model does not, however, limit the dual oxidase's peroxidase domain from other activities that might make the paired enzymes more versatile, such as protein cross-linking (Edens et al., 2001).

The maternal pool of Udx1 transcript in zygotes and the reserve pool of Udx1 protein in granules not associated with the primary, fertilization-activated population at the egg cortex suggest that this protein may be utilized later in embryogenesis. One possible role for this enzyme is as a source of cell signaling downstream of calcium. Reactive oxygen species, particularly H_2O_2, have recently been identified as essential molecules involved with autocrine and paracrine signaling (Kamata and Hirata, 1999; Neill et al., 2002), particularly in cell cycle regulation (Nasr-Esfahani et al., 1990; Chen et al., 2004) and proliferation (Burdon, 1995; Stone and Collins, 2002). Given that calcium transients are necessary for passage through mitosis and differentiation (Browne et al., 1996; Whitaker and Larman, 2001; Yazaki et al., 2004), we postulate that the oxidase activity of Udx1 may also play an active role in triggering H_2O_2-dependent signaling during embryogensis. Regulation of oxidase activity would most likely occur through the dual oxidase's paired EF-hand domains that are most identical to the visinin-like protein subfamily of neuronal calcium sensing proteins, such as neurocalcin and hippocalcin (Braunewell and Gundelfinger, 1999). Calcium sensor proteins in this calmodulin-like subfamily display free calcium affinities in the low nanomolar to micromolar concentrations and interact with other signaling proteins through hydrophobic residues exposed upon calcium chelation (Skelton et al., 1994; Kawasaki et al., 1998). Therefore, multiple mechanisms would ensure that H_2O_2 synthesis never achieves the same flurry as the oxidative burst at fertilization: catalase activity of Udx1, low intracellular calcium concentrations (Whitaker and Larman, 2001; Yazaki et al., 2004), constitutively elevated cytosolic pH_i (Dube et al., 1985; Baltz, 1993), and regulation by PKC could all serve to modulate local concentrations of H_2O_2. In turn, localized or prolonged exposure to low concentrations of H_2O_2 may act to stimulate specific cell signaling cascades (Kamata and Hirata, 1999; Blanchetot et al., 2002; Maulik and Das, 2002).

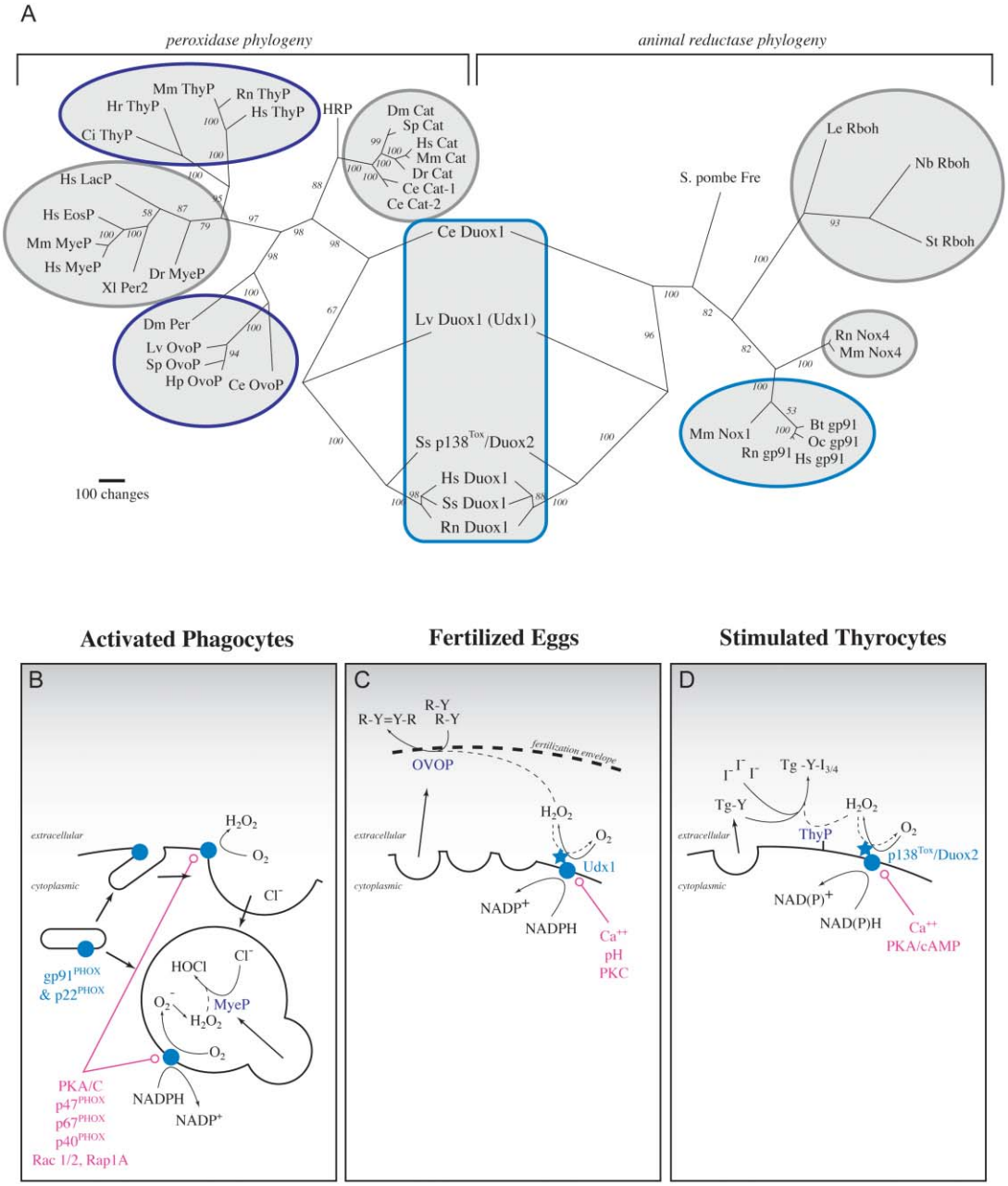

Figure 7. Comparison of Different Peroxidase-NAD(P)H Oxidase Systems

(A) Unrooted phylogram of peroxidase (left) and animal reductase (right) domains of dual oxidases compared to single-domain enzymes. Numbers are bootstrap values for each node. Class colors correspond to specific enzymatic modules (B–D). Bt, *B. taurus*; Ce, *C. elegans*; Ci, *C. intestinalis*; Dr, *D. rerio*; Dm, *D. melanogaster*; Hr, *H. roretzi*; Hs, *H. sapiens*; Le, *L. esculentum*; Lv, *L. variegatus*; Mm, *M. musculus*; Nb, *N. benthamiana*; Oc, *O. cuniculus*; Rn, *R. norvegicus*; *S. pombe*, *S. pombe*; St, *S. tuberosum*; Ss, *S. scrofa*. Cat/CTL, catalase; Duox, dual oxidase; EosP, eosinophil peroxidase; FRE, ferric reductase (yeast); gp91, gp91^{PHOX} homolog; HRP, horseradish peroxidase; LacP, lactoperoxidase; MyeP, myeloperoxidase; NOX, NADPH oxidase family member; OvoP, ovoperoxidase; Per, peroxidase; Rboh, respiratory burst oxidase homolog.

(B) Neutrophil cytochrome b_{558}-myeloperoxidase system.

(C) Sea urchin egg Udx1-ovoperoxidase machinery.

(D) Thyroid NAD(P)H oxidase-thyroid peroxidase system.

Abbreviations: PKC, protein kinase C; R-Y, extracellular matrix protein with a reactive tyrosine residue; cAMP, cyclic adenosine monophosphate; PKA, protein kinase A; Tg-Y, thyroglobulin with a reactive tyrosine residue; p138^{Tox}/Duox2, thyroid NADPH oxidase/dual oxidase. H_2O_2, hydrogen peroxide; NAD(P)$^+$/H, nicotinamide adenine dinucleotide (phosphate) in oxidized (-$^+$) and reduced (-H) forms. For dual oxidases, note the peroxidase domain (star) is distinct from the generic animal reductase domain (circle). For details, see Babior (1999) and Dunn and Dunn (2001).

A survey of the heme peroxidase family identifies a cluster of ovoperoxidase-like homologs in many invertebrates (Figure 7A; Daiyasu and Toh, 2000). In the sea urchin, this protein is expressed exclusively during oogenesis (LaFleur et al., 1998) and requires H_2O_2 synthesis to cross-link the FE constituents (Hall, 1978; Showman and Foerder, 1979). Peroxidase activity has also been identified in the oocytes and eggs of many other species at fertilization: in mouse cortical granules and to the outer surface of the zona pellucida (Gulyas and Schmell, 1980), in the fertilization capsule of *Discoglossus pictus* (Pitari et al., 1993), in the chorion of the fish *Tribolodon hakonensis* (Kudo, 1988), and in the eggshells of mosquitoes (Li et al., 1996). Each of these peroxidases requires a source of H_2O_2. Extrapolating from observations here, as well as the century-old history of the "respiratory burst" at fertilization in sea urchins, we postulate that a similar dual oxidase-dependent mechanism is functional at fertilization throughout phylogeny.

Experimental Procedures

Animals

Strongylocentrotus purpuratus and *Lytechinus variegatus* gametes were obtained and handled as previously described (Wong and Wessel, 2004).

Quantitation of Hydrogen Peroxide Synthesis Dynamics In Situ Using an Imaging Photon Detector

Keihart chambers (Keihart, 1982) were loaded with artificial seawater (ASW) containing approximately 100 eggs and 100 μM luminol (diluted from a 10 mM stock made up in 100 mM K_2CO_3 [pH 11.5]). Hydrogen peroxide (H_2O_2) production by fertilized eggs was imaged via photons emitted from luminol conjugation (Créton and Jaffe, 2001), using an Axiovert 100TV microscope (Zeiss, Thornwood, NY) equipped with an imaging photon detector (Photek, East Sussex, UK). Photon generation was acquired over a 12 min period at 23°C. Brightfield images were taken at the beginning and end of acquisitions. Recording and analysis of photon generation per zygote were made using IpdWin95 software (Sciencewares, East Falmouth, MA).

Oxidative burst activity in individual zygotes was quantified by analysis of traces generated for circular areas over each embryo. 70 s before the 20% maximum amplitude measurement was arbitrarily designated as the trace start time. All further "detected" data were gathered based on the 20%, 50%, and 80% of maximum amplitudes, and total photons were calculated by curve integration (see Figure 1C). Detected data were corrected for photon loss within the objective and the detector using an optical (×12) and calibration (×33.3) conversion factor (Créton and Jaffe, 2001), yielding the absolute number of photons emitted per zygote. The quantum efficiency of luminol (1.24%) was used to translate absolute photon counts to actual molecules of H_2O_2 (Créton and Jaffe, 2001). Normalizations for surface area and volume were made using the assumption that the zygote and its FE are perfect spheres.

Fluorometric Population Kinetics Assays

Approximately 100 eggs in ASW were loaded into triplicate wells of a 96-well plate, containing 2 μl of sperm, A23187 (10 mg/ml; Sigma, St. Louis, MO), ASW, or DMSO. The final 200 μl reaction volumes contained 50 μM Amplex Red (Molecular Probes, Eugene, OR) and 20 units of horseradish peroxidase (Sigma). An Ascent Fluoroskan fluorimeter was used to measure kinetics of resorufin formation by proprietary software (Labsystems, Franklin, MA). Kinetic readings were taken with a 530 nm excitation-590 nm emission filter pair every 30 s over 15 min. Average linear rates per well were calculated from data points generated over 210 s (points 8–31). The population in each well exhibited greater than 90% FE formation. Data were normalized by subtracting the average rate of resorufin formation of the triplicate unfertilized (ASW)/unactivated (DMSO) wells from triplicate fertilized (sperm)/activated (A23187) wells.

Egg Fractionation

Eggs were fractionated, as described, into cell surface complex (Kinsey, 1986), yolk (Brooks and Wessel, 2002), and cytosol (supernatant from a 10,000 × g, 10 min centrifugation of homogenate). All samples were isolated in isotonic, calcium-free buffer (0.5 M NaCl, 0.01 M KCl, 1.5 mM $NaHCO_3$, 60 mM NaOH, 20 mM EGTA [pH 8.0]) in the presence of Complete Mini EDTA-free Protease Inhibitor Cocktail (1 tablet per 10 ml ASW; Roche, Indianapolis, IN). Aliquots were stored at 4°C and used within 5 days.

Fluorometric Egg Fraction Kinetic Assays

Egg fractions were tested for H_2O_2 generation using Amplex Red (Molecular Probes) conversion to resorufin, as above on live eggs. Egg fractions were diluted in calcium-free activity buffer (CFAB; 0.5 M NaCl, 10 mM KCl, 2.5 mM $NaHCO_3$, 60 mM NaOH, 10 mM $MgCl_2$, 1 mM EGTA, 100 mM HEPES [pH 6.8]). The final pH of this CFAB was adjusted for a 0.2 step gradient between pH 6.4 and 7.8 for the pH titration experiment. Fractions were loaded in triplicate wells of a 96-well plate, containing 2 μl of 500 mM $CaCl_2$ or water. Then equal volumes of CFAB containing 75 μM Amplex Red (Molecular Probes), 0.002 units of horseradish peroxidase (Sigma), 100 μM NAD(P)H or equivalent oxidized cofactor (Sigma), 5×10^{-4} units of rat brain protein kinase C (Sigma), and 130 μM ATP (Sigma) topped off each reaction. Final 200 μl reactions contained one-half the final concentrations of each supplemental reagent and 0.5 μM $CaCl_2$ per well.

Loaded plates were immediately transferred to an Ascent Fluoroskan fluorimeter. Measurements were taken over 10 min using parameters as above for live eggs. The final reaction pH was measured for the pH titration experiment. The maximal linear rate over a window of 240 s (8 data points) was calculated for each reaction well. Results were normalized by first subtracting the average background rate of resorufin formation (reactions without free calcium) from calcium-activated reactions. Then the absolute background of no-sample controls (blank) was subtracted:

$$\text{Normalized rate} =$$

$$(\text{rate}_{\text{activated}} - \text{rate}_{\text{background}})_{\text{sample}} - (\text{rate}_{\text{activated}} - \text{rate}_{\text{background}})_{\text{blank}}.$$

Two-tailed Student t tests were used to compare sample sets.

Inhibitors

Stocks (100×) in appropriate solvents (dimethylsulfoxide [DMSO] or an aqueous buffer) were made of the following inhibitors: diphenyleneiodonium (DPI), apocynin (Apo), acetosyringone (Aceto), rottlerin, 3-amino-triazole (Sigma), staurosporine (Kamiya Biomedical Co., Seattle, WA), or myristoylated PKC pseudosubstrate peptide 20-28 (EMD Bioscience, San Diego, CA). Samples were preincubated in 1× solutions of each inhibitor for 10 min before assaying. Experimental results using inhibitors are reported as percentage of solvent control (0 μM).

Cloning and Sequencing

Nested primers were designed against a single thyroid oxidase exon (BAC SP_0004_A2_F05_SP6E; http://sugp.caltech.edu), and the amplicons were used to hybridization screen an *L. variegatus* λZAP ovary cDNA libraries as described (Wong and Wessel, 2004). All nucleotide and amino acid positions of the contig deposited in GenBank (AY747667) are reported from A = 1 of the predicted ATG initiation codon or methionine.

RNA Analysis

RNA gel blot analysis was performed as described (Bruskin et al., 1981). For in situ hybridization, a 362 bp PCR amplicon spanning nucleotides 2573 to 2935 was subcloned into pGEM-T easy (Promega Corp., Madison, WI). RNA probes were synthesized from the T7 and Sp6 promoters (Megascript kits; Ambion Inc., Austin, TX) with digoxigenin-UTP (Roche). In situ hybridizations (Ransick et al., 1993) included two washes with xylene following the initial dehydration. Samples were imaged by Nomarski light microscopy using an Orca CCD camera (Hammamatsu Corp., Bridgewater, NJ) on an AxioPlan microscope (Zeiss), controlled by Metamorph software (Universal Imaging Co., Downingtown, PA).

Reverse Transcriptase Polymerase Chain Reactions

Single-tube multiplex RT-PCR reactions were run using the Access RT-PCR kit (Promega Corp.). Ten *L. variegatus* oocytes, eggs, or zygotes were lysed (Voronina et al., 2003), and then two-cell equivalents were used as template in each 50 μl RT-PCR reaction to probe for three products: a 362 bp *L. variegatus* dual oxidase product starting at position 2574 (50 pmol each primer: forward 5′-ACTT GACTTCGACGCTGATG; reverse 5′-AGTTTGTCAAGGTCCGTCTC); a 266 bp *L. variegatus* cortical granule control product from SFE9 (12.5 pmol each primer: forward 5′-GTATTCGGGACTGTCCTTC; reverse 5′- CTTCACCATTCACTGGACAC); and a 192 bp control product from *L. variegatus* 18S RNA (1 pmol each primer: forward 5′-TAGGACCTCGGTTCTATTGC; reverse 5′-TATCTGATCGCCTTCG AACC). Each multiplex RT-PCR reaction was processed for 1 hr at 48°C, 95°C for 5 min, and then 45 cycles of 95°C for 30 s, 55°C for 1 min, 68°C for 2 min. One-fifth of the reaction was separated on a 2% agarose gel, stained with ethidium bromide, and imaged on a Typhoon fluorescent scanner (Amersham Biosciences, Piscataway, NJ).

Polyclonal Antibody Analysis

Antiserum was raised in rabbits against three independent regions of the dual oxidase expressed from pQE vectors (Qiagen, Chatsworth, CA): anti-peroxidase, residues 26 to 655 (NTAST…MEPCT); anti-bridge, residues 553 to 1221 (LMETT…FSVMH); and anti-NADPH, residues 1345 to 1624 (RKKAE…HHFEN). All recombinant proteins were overexpressed in *Escheria coli*, purified by nickel-column chromatography, and injected as described (Wong and Wessel, 2004).

Antibodies were affinity-purified using immunogen bound to Affigel-10 or 15 beads (BioRad, Hercules, CA). Preimmune IgGs were purified using Protein A-sepharose beads (Sigma). Elutions were equilibrated to an application-appropriate buffer. Equal masses of each affinity-purified antibodies, or equivalent total mass of preimmune antibodies, were used per experiment, unless otherwise noted.

Immunoblot analysis and immunofluorescence localization were performed as described (Wong and Wessel, 2004). Whole-mount fluorescence images were generated by merging six images acquired in z-stacks, spanning equal distances above and below the cell equator (total of 10 μm for *L. variegatus* and 5 μm for *S. purpuratus*), to produce the final image.

Antibody Functional Blocking Studies

Affinity-purified or preimmune antibodies equilibrated to CFAB (see above) were preincubated with cell surface complex for 30 min prior to assaying in vitro effects. All other parameters were as above for egg fraction kinetic assays. All antibody inhibition is reported as percentage of preimmune control.

In vivo antibody studies tested affinity-purified anti-NADPH or preimmune antibodies (see above) equilibrated to 50 mM KCl by buffer exchange. Fluorophore-conjugated Dextran (10,000 MW) was added to give a final concentration of 2 mM Dextran conjugate and 2.5 mg/ml antibody. Anti-NADPH injection solutions contained Texas red Dextran (Molecular Probes); preimmune injection solutions contained both Texas red Dextran and AlexaFluor 488 Dextran (Molecular Probes).

L. variegatus eggs were injected with antibody solution using a PLI-100 pressure injector (Harvard Apparatus, Holliston, MA) set up on an Axiovert 25c microscope (Zeiss). After a 30 min recovery period, mixes of injected and uninjected control eggs were transferred from the injection chamber to a modified Keihart chamber filled with 100 μM luminol in ASW. This chamber was moved to the Axiovert 100TV microscope to measure H_2O_2 production per zygote using the IPD (see above), imaging over a 20 min period. Chambers were then moved to an Axiovert 200M miscroscope (Zeiss) to image fluorophore content using a CoolSnap HQ CCD camera (Roper Scientific, Duluth, GA) driven by Metamorph software.

Successful fertilizations were scored by the presence of a FE. Mass of antibody injected per zygote was estimated by Texas red fluorescence and then normalized ratiometrically to autofluorescence of uninjected zygotes. Preimmune injections were identified by AlexaFluor488 fluorescence. Calibrations for the final antibody concentration in the egg were calculated from the ratio of injection volumes versus egg volume. The average photon emission rate (total photons divided by duration of burst) was calculated per zygote and plotted as a percentage of uninjected control.

Analysis of Fertilization Envelope Phenotypes

The susceptibility of FEs to mechanical and chemical treatment (Harvey, 1909; Hall, 1978) was used to identify the cross-linking phenotype. Pliability of FEs was tested mechanically using a turbulence assay: at 20 min postinsemination, cells were resuspended to a final volume of 600 μl in microfuge tubes and then inverted at 8 rotations per minute for 30 min. Chemical sensitivity of FEs was assayed by adding an equal volume of 12 N HCl or 20 mM dithiothreitol (DTT; Sigma) per reaction 20 min postinsemination. Over 300 zygotes per treatment were scored for the presence of a visible FE.

Localization and Quantification of Dityrosine Cross-Link Formation

Quantitation of peroxidase-mediated catalysis of dityrosine cross-link formation within the FE was achieved with the fluorescent conjugate tyramide-AlexaFluor488 (Molecular Probes; Gross, 1959; Hunyady et al., 1996). Stock solution (see manufacturer handbook) of tyramide-AlexaFluor488 was added at 1:200 dilution before insemination. 20 min after insemination, eggs were washed twice with ASW and then resuspended in a 0.5% solution of formalin in ASW. Incorporated AlexaFluor488 was imaged on an LSM410 controlled by Renaissance 4.10 software. Fluorescence intensity at the FE equator was quantitated with Metamorph software and normalized to cross-sectional area. Mean values from 12 to 15 individual zygotes per species per treatment are reported.

Quantitation of Endogenous Cross-Linking by Fel Electrophoresis

15 μg of homogenized zygotes (20 min postinsemination) were immunoblotted (see above), probed for SFE9 (Wessel, 1995) and YP30 (Wessel et al., 2000), and then detected with Cy3-conjugated, affinity-purified goat anti-rabbit IgG (Molecular Probes). Fluorescence was visualized with a Typhoon fluorescent scanner. Band intensities were quantitated using ImageQuant software (Amersham Biosciences) and SFE9 values were normalized to YP30 values per treatment.

Phylogenetic Analysis

Phylogeny of the dual oxidase and its closest enzymatic relatives was determined by aligning the translated open reading frames of each candidate in MacVector (Accelrys, Burlington, MA). Extraneous residues in one sequence, consisting of less than 2% of the alignments, were ignored during analysis in PAUP (Swofford, 2002). The most parsimonious relationship was obtained independently for the peroxidase and reductase domains. Heuristic searches were performed using the default TBR branch-swapping algorithm, and bootstrap scores were calculated from over 500 reiterations to measure confidence levels for specific pairing. Sequences used for comparison are listed (Supplemental Figure S3).

Acknowledgments

We would like to thank Drs. Sam Beale, Luiza Nogaj, Jill Kreiling, and members of PRIMO for their important insights and critical feedback. We gratefully acknowledge support from the NIH Research Training Grant (J.L.W.), the NSF (R.C.), and the NIH and NSF (G.M.W.).

Received: July 26, 2004
Revised: September 19, 2004
Accepted: September 29, 2004
Published: December 6, 2004

References

Babior, B.M. (1999). NADPH oxidase: an update. Blood *93*, 1464–1476.

Baltz, J.M. (1993). Intracellular pH regulation in the early embryo. Bioessays *15*, 523–530.

Bass, D.A., DeChatelet, L.R., Burk, R.F., Shirley, P., and Szejda, P. (1977). Polymorphonuclear leukocyte bactericidal activity and oxidative metabolism during glutathione peroxidase deficiency. Infect. Immun. *18*, 78–84.

Blanchetot, C., Tertoolen, L.G., and den Hertog, J. (2002). Regulation of receptor protein-tyrosine phosphatase alpha by oxidative stress. EMBO J. *21*, 493–503.

Boldt, J., Schuel, H., Schuel, R., Dandeckar, P.V., and Troll, W. (1981). Reaction of sperm with egg-derived hydrogen peroxide helps prevent polyspermy during fertilization in the sea urchin. Gamete Res. *4*, 365–377.

Braunewell, K.H., and Gundelfinger, E.D. (1999). Intracellular neuronal calcium sensor proteins: a family of EF-hand calcium-binding proteins in search of a function. Cell Tissue Res. *295*, 1–12.

Brooks, J.M., and Wessel, G.M. (2002). The major yolk protein in sea urchins is a transferrin-like, iron binding protein. Dev. Biol. *245*, 1–12.

Browne, C.L., Créton, R., Karplus, E., Mohler, P.J., Palazzo, R.E., and Miller, A.L. (1996). Analysis of the calcium transient at NEB during the first cell cycle in dividing sea urchin eggs. Biol. Bull. *191*, 5–16.

Bruskin, A.M., Tyner, A.L., Wells, D.E., Showman, R.M., and Klein, W.H. (1981). Accumulation in embryogenesis of five mRNAs enriched in the ectoderm of the sea urchin pluteus. Dev. Biol. *87*, 308–318.

Burdon, R.H. (1995). Superoxide and hydrogen peroxide in relation to mammalian cell proliferation. Free Radic. Biol. Med. *18*, 775–794.

Chance, B. (1949). The properties of the enzyme-substrate compounds of peroxidase and peroxides. I. The spectra of the primary and secondary complexes. Arch. Biochem. Biophys. *21*, 416–430.

Chandler, D.E., and Heuser, J. (1980). The vitelline layer of the sea urchin egg and its modification during fertilization. A freeze-fracture study using quick-freezing and deep-etching. J. Cell Biol. *84*, 618–632.

Chen, K.C., Zhou, Y., Xing, K., Krysan, K., and Lou, M.F. (2004). Platelet derived growth factor (PDGF)-induced reactive oxygen species in the lens epithelial cells: the redox signaling. Exp. Eye Res. *78*, 1057–1067.

Coburn, M., Schuel, H., and Troll, W. (1981). A hydrogen peroxide block to polyspermy in the sea urchin *Arbacia punctulata*. Dev. Biol. *84*, 235–238.

Créton, R., and Jaffe, L.F. (2001). Chemiluminescence microscopy as a tool in biomedical research. Biotechniques *31*, 1098–1100, 1102–1095.

Daiyasu, H., and Toh, H. (2000). Molecular evolution of the myeloperoxidase family. J. Mol. Evol. *51*, 433–445.

Deits, T.L., and Shapiro, B.M. (1986). Conformational control of ovoperoxidase catalysis in the sea urchin fertilization membrane. J. Biol. Chem. *261*, 12159–12165.

Deits, T., Farrance, M., Kay, E.S., Medill, L., Turner, E.E., Weidman, P.J., and Shapiro, B.M. (1984). Purification and properties of ovoperoxidase, the enzyme responsible for hardening the fertilization membrane of the sea urchin egg. J. Biol. Chem. *259*, 13525–13533.

Dube, F., Schmidt, T., Johnson, C.H., and Epel, D. (1985). The hierarchy of requirements for an elevated intracellular pH during early development of sea urchin embryos. Cell *40*, 657–666.

Dunn, J.T., and Dunn, A.D. (2001). Update on intrathyroidal iodine metabolism. Thyroid *11*, 407–414.

Dupuy, C., Deme, D., Kaniewski, J., Pommier, J., and Virion, A. (1988). Ca^{2+} regulation of thyroid NADPH-dependent H_2O_2 generation. FEBS Lett. *233*, 74–78.

Edens, W.A., Sharling, L., Cheng, G., Shapira, R., Kinkade, J.M., Lee, T., Edens, H.A., Tang, X., Sullards, C., Flaherty, D.B., et al. (2001). Tyrosine cross-linking of extracellular matrix is catalyzed by Duox, a multidomain oxidase/peroxidase with homology to the phagocyte oxidase subunit gp91phox. J. Cell Biol. *154*, 879–891.

Eichholtz, T., de Bont, D.B., de Widt, J., Liskamp, R.M., and Ploegh, H.L. (1993). A myristoylated pseudosubstrate peptide, a novel protein kinase C inhibitor. J. Biol. Chem. *268*, 1982–1986.

Ekholm, R., and Bjorkman, U. (1997). Glutathione peroxidase degrades intracellular hydrogen peroxide and thereby inhibits intracellular protein iodination in thyroid epithelium. Endocrinology *138*, 2871–2878.

Fahey, R.C., Mikolajczyk, S.D., Meier, G.P., Epel, D., and Carroll, E.J., Jr. (1976). The glutathione thiol-disulfide status in the sea urchin egg during fertilization and the first cell division cycle. Biochim. Biophys. Acta *437*, 445–453.

Foerder, C.A., and Shapiro, B.M. (1977). Release of ovoperoxidase from sea urchin eggs hardens the fertilization membrane with tyrosine crosslinks. Proc. Natl. Acad. Sci. USA *74*, 4214–4218.

Foerder, C.A., Klebanoff, S.J., and Shapiro, B.M. (1978). Hydrogen peroxide production, chemiluminescence, and the respiratory burst of fertilization: interrelated events in early sea urchin development. Proc. Natl. Acad. Sci. USA *75*, 3183–3187.

Gross, A.J. (1959). The oxidation of tyramine, tyrosine, and related compounds by peroxidase. J. Biol. Chem. *234*, 1611–1614.

Gschwendt, M., Muller, H.J., Kielbassa, K., Zang, R., Kittstein, W., Rincke, G., and Marks, F. (1994). Rottlerin, a novel protein kinase inhibitor. Biochem. Biophys. Res. Commun. *199*, 93–98.

Gulyas, B.J., and Schmell, E.D. (1980). Ovoperoxidase activity in ionophore-treated mouse eggs. I. Electron microscopic localization. Gamete Res. *3*, 267–278.

Haley, S.A., and Wessel, G.M. (1999). The cortical granule serine protease CGSP1 of the sea urchin, *Strongylocentrotus purpuratus*, is autocatalytic and contains a low-density lipoprotein receptor-like domain. Dev. Biol. *211*, 1–10.

Haley, S.A., and Wessel, G.M. (2004). Proteolytic cleavage of the cell surface protein p160 is required for detachment of the fertilization envelope in the sea urchin. Dev. Biol. *272*, 191–202.

Hall, H.G. (1978). Hardening of the sea urchin fertilization envelope by peroxidase-catalyzed phenolic coupling of tyrosines. Cell *15*, 343–355.

Harvey, E.N. (1909). The mechanism of membrane formation and other early changes in developing sea urchins' eggs as bearing on the problem of artificial parthenogenesis. J. Exp. Zool. *8*, 355–376.

Heinecke, J.W., and Shapiro, B.M. (1989). Respiratory burst oxidase of fertilization. Proc. Natl. Acad. Sci. USA *86*, 1259–1263.

Heinecke, J.W., and Shapiro, B.M. (1992). The respiratory burst oxidase of fertilization. A physiological target for regulation by protein kinase C. J. Biol. Chem. *267*, 7959–7962.

Hunyady, B., Krempels, K., Harta, G., and Mezey, E. (1996). Immunohistochemical signal amplification by catalyzed reporter deposition and its application in double immunostaining. J. Histochem. Cytochem. *44*, 1353–1362.

Jaffe, L.A., Giusti, A.F., Carroll, D.J., and Foltz, K.R. (2001). Ca^{2+} signalling during fertilization of echinoderm eggs. Semin. Cell Dev. Biol. *12*, 45–51.

Johnson, C.H., and Epel, D. (1981). Intracellular pH of sea urchin eggs measured by the dimethyloxazolidinedione (DMO) method. J. Cell Biol. *89*, 284–291.

Kamata, H., and Hirata, H. (1999). Redox regulation of cellular signalling. Cell. Signal. *11*, 1–14.

Kawasaki, H., Nakayama, S., and Kretsinger, R.H. (1998). Classification and evolution of EF-hand proteins. Biometals *11*, 277–295.

Keihart, D.P. (1982). Microinjection of echinoderm eggs: apparatus and procedures. In Methods in Cell Biology, D.M. Prescott, ed. (Orlando, FL: Academic Press), pp. 13–31.

Kimura, T., Van Keymeulen, A., Golstein, J., Fusco, A., Dumont, J.E., and Roger, P.P. (2001). Regulation of thyroid cell proliferation by TSH and other factors: a critical evaluation of in vitro models. Endocr. Rev. *22*, 631–656.

Kinsey, W.H. (1986). Purification and properties of the egg plasma membrane. In Methods in Cell Biology, T.E. Schroeder, ed. (Orlando, FL: Academic Press), pp. 139–152.

Klebanoff, S.J., Foerder, C.A., Eddy, E.M., and Shapiro, B.M. (1979).

Metabolic similarities between fertilization and phagocytosis. Conservation of a peroxidatic mechanism. J. Exp. Med. *149*, 938–953.

Kudo, S. (1988). Chorionic peroxidase activity in the eggs of the fish *Tribolodon hakonesis*. J. Exp. Zool. *245*, 63–70.

LaFleur, G.J., Jr., Horiuchi, Y., and Wessel, G.M. (1998). Sea urchin ovoperoxidase: oocyte-specific member of a heme-dependent peroxidase superfamily that functions in the block to polyspermy. Mech. Dev. *70*, 77–89.

Lambeth, J.D. (2002). Nox/Duox family of nicotinamide adenine dinucleotide (phosphate) oxidases. Curr. Opin. Hematol. *9*, 11–17.

Lewit-Bentley, A., and Rety, S. (2000). EF-hand calcium-binding proteins. Curr. Opin. Struct. Biol. *10*, 637–643.

Li, J., Hodgeman, B.A., and Christensen, B.M. (1996). Involvement of peroxidase in chorion hardening in *Aedes aegypti*. Insect Biochem. Mol. Biol. *26*, 309–317.

Maulik, N., and Das, D.K. (2002). Redox signaling in vascular angiogenesis. Free Radic. Biol. Med. *33*, 1047–1060.

Mellor, H., and Parker, P.J. (1998). The extended protein kinase C superfamily. Biochem. J. *332*, 281–292.

Nasr-Esfahani, M.H., Aitken, J.R., and Johnson, M.H. (1990). Hydrogen peroxide levels in mouse oocytes and early cleavage stage embryos developed in vitro or in vivo. Development *109*, 501–507.

Neill, S., Desikan, R., and Hancock, J. (2002). Hydrogen peroxide signalling. Curr. Opin. Plant Biol. *5*, 388–395.

Nomura, K., and Suzuki, N. (1995). Sea urchin ovoperoxidase: solubilization and isolation from the fertilization envelope, some structural and functional properties, and degradation by hatching enzyme. Arch. Biochem. Biophys. *319*, 525–534.

O'Donnell, B.V., Tew, D.G., Jones, O.T., and England, P.J. (1993). Studies on the inhibitory mechanism of iodonium compounds with special reference to neutrophil NADPH oxidase. Biochem. J. *290*, 41–49.

Pitari, G., Dupre, S., Fusco, C., Maurizi, G., and Campanella, C. (1993). Jelly plug dissolution in *Discoglossus pictus* eggs (Anura) involves peroxidase-like activity and oxidative opening of disulphide bonds. Zygote *1*, 61–69.

Pullar, J.M., Vissers, M.C., and Winterbourn, C.C. (2000). Living with a killer: the effects of hypochlorous acid on mammalian cells. IUBMB Life *50*, 259–266.

Ransick, A., Ernst, S., Britten, R.J., and Davidson, E.H. (1993). Whole mount in situ hybridization shows Endo 16 to be a marker for the vegetal plate territory in sea urchin embryos. Mech. Dev. *42*, 117–124.

Schomer, B., and Epel, D. (1998). Redox changes during fertilization and maturation of marine invertebrate eggs. Dev. Biol. *203*, 1–11.

Schuel, H., and Schuel, R. (1986). Sea urchin sperm peroxidase is competitively inhibited by benzohydroxamic acid and phenylhydrazine. Biochem. Cell Biol. *64*, 1333–1338.

Schwarzer, C., Machen, T.E., Illek, B., and Fischer, H. (2004). NADPH oxidase-dependent acid production in airway epithelial cells. J. Biol. Chem. *279*, 36454–36461.

Shapiro, B.M., Somers, C.E., and Weidman, P.J. (1989). Extracellular remodeling during fertilization. In The Cell Biology of Fertilization, H. Schatten and G. Schatten, eds. (San Diego, CA: Academic Press).

Shen, S.S. (1995). Mechanisms of calcium regulation in sea urchin eggs and their activities during fertilization. Curr. Top. Dev. Biol. *30*, 63–101.

Shen, S.S., and Steinhardt, R.A. (1978). Direct measurement of intracellular pH during metabolic derepression of the sea urchin egg. Nature *272*, 253–254.

Shen, S.S., and Steinhardt, R.A. (1979). Intracellular pH and the sodium requirement at fertilisation. Nature *282*, 87–89.

Showman, R.M., and Foerder, C.A. (1979). Removal of the fertilization membrane of sea urchin embryos employing aminotriazole. Exp. Cell Res. *120*, 253–255.

Skelton, N.J., Kordel, J., Akke, M., Forsen, S., and Chazin, W.J. (1994). Signal transduction versus buffering activity in Ca(2+)-binding proteins. Nat. Struct. Biol. *1*, 239–245.

Somers, C.E., Battaglia, D.E., and Shapiro, B.M. (1989). Localization and developmental fate of ovoperoxidase and proteoliaisin, two proteins involved in fertilization envelope assembly. Dev. Biol. *131*, 226–235.

Stone, J.R., and Collins, T. (2002). The role of hydrogen peroxide in endothelial proliferative responses. Endothelium *9*, 231–238.

Swofford, D.L. (2002). PAUP*: Phylogenetic Analysis Using Parsimony (* and Other Methods). Version 4 edn (Sunderland, MA: Sinauer Associates).

Takahashi, A., Totsune-Nakano, H., Nakano, M., Mashiko, S., Suzuki, N., Ohma, C., and Inaba, H. (1989). Generation of O2- and tyrosine cation-mediated chemiluminescence during the fertilization of sea urchin eggs. FEBS Lett. *246*, 117–119.

Tamaoki, T., Nomoto, H., Takahashi, I., Kato, Y., Morimoto, M., and Tomita, F. (1986). Staurosporine, a potent inhibitor of phospholipid/Ca++dependent protein kinase. Biochem. Biophys. Res. Commun. *135*, 397–402.

Turner, E., Klevit, R., Hopkins, P.B., and Shapiro, B.M. (1986). Ovothiol: a novel thiohistidine compound from sea urchin eggs that confers NAD(P)H-O2 oxidoreductase activity on ovoperoxidase. J. Biol. Chem. *261*, 13056–13063.

Turner, E., Hager, L.J., and Shapiro, B.M. (1988). Ovothiol replaces glutathione peroxidase as a hydrogen peroxide scavenger in sea urchin eggs. Science *242*, 939–941.

Van den Worm, E., Beukelman, C.J., Van den Berg, A.J., Kroes, B.H., Labadie, R.P., and Van Dijk, H. (2001). Effects of methoxylation of apocynin and analogs on the inhibition of reactive oxygen species production by stimulated human neutrophils. Eur. J. Pharmacol. *433*, 225–230.

Voronina, E., Marzluff, W.F., and Wessel, G.M. (2003). Cyclin B synthesis is required for sea urchin oocyte maturation. Dev. Biol. *256*, 258–275.

Wang, Y.X., Poon, C.I., Poon, K.S., and Pang, C.C. (1993). Inhibitory actions of diphenyleneiodonium on endothelium-dependent vasodilatations in vitro and in vivo. Br. J. Pharmacol. *110*, 1232–1238.

Warburg, O. (1908). Beobachtungen uber die Oxydationsprozesse im Seeigelei. Z Physiol Chem *57*, 1–16.

Ward, N.E., and O'Brian, C.A. (1993). Inhibition of protein kinase C by N-myristoylated peptide substrate analogs. Biochemistry *32*, 11903–11909.

Wendl, T., Lun, K., Mione, M., Favor, J., Brand, M., Wilson, S.W., and Rohr, K.B. (2002). Pax2.1 is required for the development of thyroid follicles in zebrafish. Development *129*, 3751–3760.

Wessel, G.M. (1995). A protein of the sea urchin cortical granules is targeted to the fertilization envelope and contains an LDL-receptor-like motif. Dev. Biol. *167*, 388–397.

Wessel, G.M., Zaydfudim, V., Hsu, Y.J., Laidlaw, M., and Brooks, J.M. (2000). Direct molecular interaction of a conserved yolk granule protein in sea urchins. Dev. Growth Differ. *42*, 507–517.

Wessel, G.M., Brooks, J.M., Green, E., Haley, S., Voronina, E., Wong, J., Zaydfudim, V., and Conner, S. (2001). The biology of cortical granules. Int. Rev. Cytol. *209*, 117–206.

Whalley, T., Terasaki, M., Cho, M.S., and Vogel, S.S. (1995). Direct membrane retrieval into large vesicles after exocytosis in sea urchin eggs. J. Cell Biol. *131*, 1183–1192.

Whitaker, M., and Larman, M.G. (2001). Calcium and mitosis. Semin. Cell Dev. Biol. *12*, 53–58.

Wong, J.L., and Wessel, G.M. (2004). Major components of a sea urchin block to polyspermy are structurally and functionally conserved. Evol. Dev. *6*, 134–153.

Yazaki, I., Abe, M., Santella, L., and Koyama, Y. (2004). Mechanisms of calcium elevation in the micromeres of sea urchin embryos. Biol. Cell. *96*, 153–167.

Yip, C.C. (1966). The iodination of tyrosine by myeloperoxidase and beef thyroids: the possible involvement of free radicals. Biochim. Biophys. Acta *122*.